Mechanical response of UO2 single crystals submitted to low-energy ion irradiation

Tien-Hien Nguyen, Aurélien Debelle, Alexandre Boulle, Frédérico Garrido, Lionel Thomé, Valérie Demange

Mechanical response of UO_2 single crystals submitted to low-energy ion irradiation

Tien-Hien Nguyen[a,b], Aurélien Debelle[a], Alexandre Boulle[c], Frédérico Garrido[a], Lionel Thomé[a], Valérie Demange[d]

a. Centre de Sciences Nucléaires et de Sciences de la Matière (CSNSM),

Univ. Paris-Sud – CNRS/IN2P3, Université Paris-Saclay, Bâtiment 108, 91405 Orsay Cedex, France

b. Department of Physics, Vietnam National University of Agriculture, Trau Quy, Gia Lam, Hanoi, Vietnam

c. Science des Procédés Céramiques et de Traitements de Surface CNRS UMR 7315, Centre Européen de la Céramique, 12 rue Atlantis, 87068 Limoges, France

d. Institut des Sciences Chimiques de Rennes, CNRS UMR 6226, 263 avenue du Général Leclerc, Campus de Beaulieu - Bâtiment 10B, 35042 Rennes Cedex, France

Abstract

{111}- and {100}-oriented UO_2 single crystals were irradiated with 500-keV Ce^{3+} ions in the 10^{14} - $9x10^{14}$ cm^{-2} fluence range. The irradiation-induced strain was monitored using high-resolution X-ray diffraction. A mechanical modelling dedicated to thin irradiated layers was applied to account for the reaction of the unirradiated part of the crystals. The elastic strain, which is confined along the surface normal of the samples, increases with ion fluence until it is dramatically relieved. This behaviour is observed for both orientations. While the measured elastic strain depends on the crystallographic direction, the strain due to irradiation defects only is found to be equal for both directions, with a maximum value of ~0.5%. Strain relaxation takes place at the damage peak, but the in-plane lattice parameter of the irradiated layer remains unchanged and equal to that of the pristine material. Meanwhile, the strain at the damaged/pristine interface continues to increase.

Keywords: XRD; UO_2; radiation effects; elastic strain; defects;

PACS: 61.05.cp; 61.80.Jh; 61.72.J-; 61.72.Dd; 62.20.D-

Introduction

Uranium dioxide is the standard nuclear fuel used in modern, conventional power reactors. This material must then face irradiation by various energetic particles, which includes fission fragments, alpha particles and neutrons. It has therefore to resist to these severe conditions, because irradiation is inevitably concomitant with defect production, thereby potentially inducing drastic structural or microstructural modifications that may eventually lead to the loss of integrity of the material. One very convenient, fast, controllable and efficient way to experimentally simulate radiation damage without inserting the material inside the reactor, and thus avoiding radioactivity safety issues, is to use ion beams delivered by particle accelerators ([1,2], and see also Proceedings of the Nuclear Materials Conference, NuMat2012 and NuMat2014 in J. Nucl. Mater.). Varying the nature, energy, fluence and dose rate, but also irradiation temperature, it is possible to selectively simulate one (or several, when using multiple ion beams) irradiation source(s).

In the case of nuclear waste disposal, after decay of the predominantly beta-decaying short-lived fission fragments, the spent fuel will be principally submitted to alpha-decay self-radiation [3]. This process will lead to helium accumulation, but also to indirect defect production due to alpha recoils. These latter are heavy, with a low energy (e.g. 70 keV Th) and therefore, their slowing down is primarily in the nuclear energy-loss regime, i.e. they are elastically scattered by screened nuclei of the target atoms. These interactions lead to collision cascades and thus to crystalline disordering. This process is sometimes refers to as the ballistic contribution to the radiation damage, by opposition to the ‘chemical’ contribution that results of the incorporation of insoluble elements; it also takes place, but to a much lesser extent, in-pile due to fission fragments at the end of their travel.

For crystalline compounds, a relevant method to monitor the irradiation-induced disorder is to measure the associated elastic strain using X-ray diffraction (XRD) [4]. However, this approach is not totally straightforward because with low-energy ion irradiation, only a shallow surface layer is altered and the bulk part of the material - which can be considered as an underlying substrate - is unaffected. A mechanical modelling was proposed by the authors to account for this particular situation. It was shown, in single-crystals, that the strain that is experimentally determined, ε^{tot}, includes two contributions: (i) the response of the irradiated, defect-containing layer ε^{def}, and (ii) the mechanical response of the undamaged part of the crystal, ε^{SR} (substrate reaction) [5-6]. It was also demonstrated that the mechanical reaction of the substrate is governed by the elastic properties of the material, and is therefore usually dependent on the crystallographic orientation [6-7]. The modelling was applied to 300-keV Cs irradiated single-crystalline cubic zirconia (ZrO_2) crystals, a material that shares the same crystallographic fluorite-type structure as UO_2, oriented along two different directions, namely <100> and <111> [6]. It must be mentioned that the dependence of the strain on the crystallographic direction has also been observed in polycrystalline 60-keV He implanted UO_2 [7]; note however that in this case, there was not only a ballistic effect during the irradiation process but also a chemical effect of the implanted He that is insoluble in almost all materials and forms He-vacancy complexes (that are precursor of He bubbles) which generate a huge elastic strain [8].

Another important result from previous studies is that in UO_2 the strain (derived from XRD measurements) [9] and the damage (determined by ion channelling analyses) build-ups occur in (at least) two steps [10-11]. In the first step, the irradiated layer responds elastically to the irradiation, and formation of defects leads to elastic strain accumulation. In the second step, a plastic relaxation of the elastic strain takes place through the formation of

extended defects. This two-step disordering process has been particularly documented in ion-irradiated cubic zirconia [12-13]. Regarding the defects formed in the second step, the following scenario was proposed: (i) interstitial point defect agglomerate and (ii) form Frank loops which grow and transform into perfect $\frac{a}{2}<110>$ dislocation loops; (iii) finally, growth of these perfect loops leads to the formation of a network of dislocation lines. This mechanism was also reported in irradiated ceria (see [14] and references therein). Both cubic zirconia and ceria can be considered as surrogate materials to urania, and it can be assumed that this scenario also holds for this material. Some work actually reported the formation of $\frac{a}{2}<110>$ dislocation loops in Kr-irradiated UO_2 single crystals [15]. Very recently, an advanced ion channelling modelling with a dedicated Monte Carlo simulation code [16] allowed to obtain a very good agreement with experimental data when involving the presence of dislocations, as a form of Rayleigh instabilities, in the damaged layers in the second step of the disordering process [11]; no particular orientation of these dislocations was used. Consequently, although there are some clues on the nature of the defects formed at high fluence, strain relaxation in the UO_2 crystals will be ascribed in the following to the formation of *extended defects*.

In our group, we are conducting a systematic study that aims at investigating the behaviour of UO_2 upon low-energy ion irradiation with different species (such as He, Xe, Ce, La), using different characterization techniques (see Ph.D. thesis [17]). In the present work, we focus on the mechanical response of UO_2 single-crystals subjected to 500 keV-Ce irradiation using high-resolution X-ray diffraction (HRXRD). These low-energy heavy ions mainly slow down in the nuclear energy-loss regime, as above explained. Furthermore, contrary to elements such as noble gases or metals (Pd, Ru…) which tend to form

precipitates, Ce (as La) is fully soluble in UO_2, meaning that it should be fully accommodated when incorporated into the urania lattice. Therefore, one may reasonably assume that chemical effects can be disregarded, and only displaced atoms during collision cascades (ballistic effects) can be considered. Both the {100} and {111} crystallographic orientations are studied, and the necessity to account for the substrate reaction is demonstrated. Moreover, the strain relaxation that occurs at high irradiation fluence is addressed.

II Experimental details

II.1. Crystal preparation and ion irradiation

{100}- and {111}-oriented UO_2 (0.3% ^{235}U) single-crystal-like samples, coming from the Joint Research Center in Ispra (Italy), were used in this study. These crystals are in fact very-high quality multi-crystals, as explained in [9] and in Section III.2 of this paper. Crystals were slice-shaped (with the crystallographic orientation determined by the Laue X-ray crystallography method), and were then mechanically polished until mirror-like finish with diamond pastes down to 0.5 µm. They were subsequently annealed at 1400°C in a mixture of H_2/Ar gases containing 10 vol. % of H_2 to assure the theoretical stoichiometry of UO_2 crystals (i.e. O/U = 2) and to remove any damage created during the polishing process. Lattice parameter of virgin samples was measured by XRD and found to be 0.547 nm. The initial crystalline quality was checked by RBS/C: measured minimum axial yields were found in good agreement with theoretical values (i.e. <2%) for pristine crystals [18]. Samples were then irradiated in the IRMA ion implanter at CSNSM-Orsay, taking care to tilt the sample holder by 7° with respect to the ion beam direction to prevent any channelling effect of the bombarding ions. Irradiations were performed at room temperature with 500-keV Ce^{3+} ions. A beam raster system was used to ensure a homogeneous irradiation over the samples'

surface. The ion flux was kept below 5×10^{11} $cm^{-2}s^{-1}$ to avoid any sample overheating. Ion fluences ranged from $\Phi = 10^{14}$ cm^{-2} up to $\Phi = 9x10^{14}$ cm^{-2}, which corresponds to concentration of incorporated element at the maximum of the distribution between ~0.012 and ~0.11 at. %, and to corresponding displacements per atom (dpa) values comprised between ~0.85 and ~7.9, as determined with the SRIM-2011 code [19] using threshold displacement energies (E_d) of 20 and 40 eV for O and U atoms, respectively. The mean projected range predicted by SRIM is ~85 nm, with a range straggling of ~40 nm. Both dpa and Ce depth profiles are presented in Fig. 1 for the $9x10^{14}$ cm^{-2} fluence.

II.2. XRD measurements

The crystals were characterized by HRXRD using a Bruker D8 laboratory diffractometer equipped with a Göbel mirror and a (4 x (220)Ge) monochromator as primary optics that allows delivering an intense, parallel and monochromatic X-ray beam (Cu $K\alpha_1$ radiation). The diffracted intensity was recorded using a 1D Lynxeye detector (192 channels covering a 2° range in 2θ) both for the reciprocal space maps (RSMs) and the ω-2θ scans (in the latter case the intensity was recorded with a single channel of the PSD which has a ~0.01° aperture). The formalism used in this paper is the one presented in [5-6,9]: (i) K_N and $K_{//}$ are the normal (out-of-plane) and parallel (in-plane) components of the scattering vector K ($2sin\theta/\lambda$), respectively; (ii) $H_{(hkl)}$ refers to the reciprocal lattice vector for the (hkl) reflection; (iii) q_N is defined as K_N-$H_{N(hkl)}$ and represents the deviation from the reciprocal lattice vector. In the following, positions on the maps are located by K_N and $K_{//}$, but also by, respectively, (i) ($-q_N/H_N$), which is equal to the elastic strain in the direction normal to the surface of implanted samples, and (ii) ($\Delta K_{//}/H_{(hkl)}$), which directly gives the width (here in degrees) of the reciprocal lattice point (RLP) in the transverse direction. For {100} crystals,

the symmetric 400 (*2θ~68.567°*) and asymmetric 402 (*2θ~78.067°)* Bragg reflections were explored, while the 222 (*2θ~58.395°*) and 331 (*2θ~75.734°*) reflections were probed for {111} crystals. Note that in all cases, the thickness probed by the X-ray beam is far larger (0.8 µm considering a 90% attenuation) than the thickness of the irradiated layer (~150 nm).

III. Results and discussion

III.1. Strain build-up

As mentioned in the Introduction, in the present irradiation conditions, elastic strain develops in the first irradiation step. In this section, attention is focused on this first step that corresponds here to ion fluences up to $7x10^{14}$ cm^{-2} (~6 dpa). Figure 2 displays symmetric ω-2θ scans recorded on irradiated {100}- (Fig. 2a) and {111}-oriented (Fig. 2b) UO_2 crystals. It is readily observed that the shape of the XRD patterns is similar for both orientations. All curves exhibit an intense narrow peak on the high-angle side, which arises from the unirradiated part of samples, and referred to as the substrate. An additional signal at lower 2θ angle is recorded for irradiated crystals, indicating that damaged layers experience a tensile elastic strain along the direction normal to the sample surface. Furthermore, this signal exhibits interference fringes that are related to the presence of a dilatation gradient [13,20]. This latter can be retrieved by fitting the XRD curves using the dynamical theory of X-ray diffraction [20]; simulations are displayed as solid lines in Figs. 2a and 2b. The corresponding strain depth profiles are presented in Fig. 3a and 3b, respectively. A detailed discussion of these profiles will be given in a forthcoming paper where strain, disorder (XRD) and damage (ion channelling) distributions will be compared. In the scope of this paper, the important finding to point out is that, though not completely identical, the strain depth profiles are almost similar for both orientations, exhibiting same trends with depth and with

increasing fluence (note also that they are equivalent to those found in the case of irradiated cubic zirconia [13]). Additionally, it must be stressed that at the highest irradiation fluence, which corresponds to the second step of the strain build-up that is discussed in the next section, XRD analyses reveal a heavily defective layer from the surface up to about 100-150 nm depth. This highly damaged layer is characterized by a large disorder level, and, as explained in [13], the elastic strain cannot be accurately determined in this region (which is why the strain profile is displayed as a dotted line). For all other ion fluences, the maximum, experimentally measured strain (ε^{tot}) is plotted as a function of both the Ce fluence and the dpa scale in Fig. 4 (full symbols). Strain is found to increase with irradiation fluence for both orientations. However, the <111>-type direction appears to be more strained than the <100>-type one, with a value of ~1.1% at $7x10^{14}$ cm^{-2} for the former and ~0.8% for the latter; this difference is significantly larger than the error bar associated to the strain values. At first, this finding seems to indicate that both crystalline orientations respond differently to ion irradiation. However, it must be reminded that ε^{tot} includes both the (triaxial) lattice swelling due to irradiation defects (ε^{def}) and an additional biaxial strain originating from the fact that the irradiated layer is laterally clamped on the substrate (the "substrate reaction", ε^{SR}). Using the modelling presented in [6], and elastic constants found in [21] (i.e. C_{11} = 396 GPa, C_{12} = 121 GPa, and C_{44} = 64 GPa), it is possible to derive ε^{def} (open symbols in Fig. 4). While the trend is obviously similar to that previously described for the total strain since both quantities are proportional, it clearly appears that the strain due to the sole defects is actually equal in the two directions. This result remains completely hidden if the mechanical behaviour of irradiated layers is not properly modelled. Furthermore, this finding indicates that ion irradiation seems to produce an equal defect concentration whatever the crystallographic orientation, assuming that same defects are produced; ion channelling

measurements reveal a similar disorder level for both orientations [17], corroborating this assumption. Total strain is larger for {111} than for {100} planes only because the elastic anisotropy factor of UO_2 is negative ($C_{44} - \frac{1}{2}(C_{11} - C_{12}) = -0.735$), meaning that the {111} planes are more compliant than the {100} ones. This property allows a larger strain to develop for a same mechanical solicitation (i.e. here a same ion fluence). At a fluence of $9x10^{14}$ cm^{-2}, the XRD curves exhibit a different shape than that observed at low fluence: the fringe pattern vanishes and instead, a diffuse signal is observed. These features hold for both crystallographic orientations, and suggest a strain relaxation, consistent with previous results [6,9].

III.2. Strain relaxation

Figure 5a depicts the scattered intensity (in logarithmic scale) in the vicinity of the 331 Bragg reflection for a UO_2 crystal irradiated at $3x10^{14}$ cm^{-2} (~2.5 dpa), *i.e.* in the first step of the damage build-up [9-11]. {331} planes make an angle Ψ=22° with respect to the {111} planes; the 331 reflection is thus asymmetric, and it must be pointed out that in this case, the normal strain is equal to $-q_N/H_{N(331)}$, where $H_{N(331)} = H_{(331)} * \cos\Psi$. In addition, since the scattering vector $K_{(331)}$ has both an in-plane and an out-of-plane component, the corresponding lattice parameters can be calculated. On this RSM, an intense signal (grey part at the top of the map) is observed at the coordinates of the unstrained (unirradiated) material, which are K_N ~ 7.388 nm^{-1} and $K_{//}$ ~ 2.985 nm^{-1}. This intense signal corresponds to the undisturbed part of the samples probed by X-rays. It is worth mentioning that several intense spots (~4) are visible at this K_N coordinate, which indicates that the non-commercial UO_2 samples used in this study are in fact multi-crystals, *i.e.* crystals composed of a few

(typically one to four) large single-crystal-like blocks very slightly inclined one with respect to another (typical disorientation angle is ~0.1°, as can be seen on the top-axis of the map in Fig. 5a); this feature has been discussed in a previous paper, and it was shown that by no means does this hamper the analysis of the XRD results [9]. Also visible on the map in Fig. 5a is a scattered intensity, emanating from the irradiated layer, spreading along the K_N direction in the region of lower values, which indicates a positive elastic strain (see also right axis of the map) along the surface normal of the crystals, in agreement with the observations of the ω-2θ scans (Figs. 2). Likewise, it is clear that the scattering vector corresponding to the irradiated region shares the same $K_{//}$ component as the underlying (unirradiated) layer, which shows that the damaged layer does not experience any in-plane strain. Such a strain state corresponds to a tetragonal distortion of the initial cubic lattice, as already observed in low-energy ion-irradiated materials [5,9,12]. The asymmetric 402 reflection of {100}-oriented UO_2 crystals irradiated at the same $9x10^{14}$ cm^{-2} fluence exhibits identical features as those observed on the map recorded for the {111}-oriented crystal (Fig. 5a), indicating that the above results hold for both orientations.

Fig. 5b displays the RSM recorded around the 331 reflection of a UO_2 crystal irradiated at $9x10^{14}$ cm^{-2} which is a fluence characteristic of the second step of the strain build-up [9-11], *i.e.* after the strain relaxation (note that the asymmetric 402 reflection of {100}-oriented UO_2 crystals irradiated at high fluence exhibit identical features). It must be remarked that three blocks are detected for this crystal, whereas four were probed in the crystal irradiated at low fluence, which leads to an excessive spreading of the scattered intensity along the $K_{//}$ direction. However, a change in the colour range can be noticed, with a more important purple-blue, low intensity component along the $K_{//}$ direction on the map corresponding to the crystal irradiated at the highest fluence. A line scan along the $K_{//}$

direction at K_N = 7.331 nm^{-1} (see grey dotted lines Figs. 5) is presented for both crystals in Fig. 6: it is clearly visible that on the curve corresponding to the crystal irradiated at 9x10^{14} cm^{-2}, there is a more gradual decrease to baseline (*i.e.* the peak tails are more pronounced) than on the curve of the crystal irradiated at 3x10^{14} cm^{-2}. In other words, the diffuse scattering is more pronounced in the crystal irradiated at high fluence. To assess this statement, the two curves were fitted with a pseudo-Voigt function (thick solid lines in Fig. 6); note that the contribution of the different blocks was not taken into account. The Lorentzian component is found to be equal to 0.6 in the curve corresponding to the sample irradiated at 9x10^{14} cm^{-2}, while it is 0.4 at 3x10^{14} cm^{-2}, consistent with the spreading of the peak tails at high fluence. More convincingly, the integral width for the peak at high fluence is nearly twice that of the peak for the crystal irradiated at low fluence (i.e. 0.012 nm^{-1} *vs.* 0.022 nm^{-1}). These findings are other evidences of the formation of extended defects associated to the strain relaxation mechanism at high fluence. What appears to be more striking is that the $K_{//}$ coordinate of the RLP corresponding to the irradiated, but (significantly) relaxed layer remains equal to that of the pristine region of the sample. This result indicates that both parts continue to share the same in-plane lattice parameter, which is that of the virgin crystal. At first glance this might seem contradictory with the observed strain relaxation. Indeed, usually, when a misfitting layer is epitaxially grown on a substrate, the increase in the associated elastic energy leads the layer to undergo strain relaxation, hence recovering its own lattice dimensions; a shift of the corresponding RLP along both K_N and $K_{//}$ is then observed (see e.g. [22]). This relaxation usually takes places during growth with the progressive generation of misfit dislocations or the formation of islands. In the present case, there is no layer growth: the irradiated layer is, since the beginning of the irradiation process, part of a bulk sample. Upon irradiation, the UO_2 lattice progressively

swells with increasing ion fluence, so that the aforementioned relaxation mechanisms cannot be activated. This explains why irradiated layers can sustain huge strain levels (up to several %, see e.g. [23,24]) as compared to grown epitaxial films. The only way for such irradiated layers to relieve the elastic energy is therefore to cancel the lattice swelling at the origin of the epitaxial strain, *i.e.* to recover its irradiation-strain-free lattice parameter; the tetragonal distortion is then simply relieved. This is a triaxial (hydrostatic) strain relaxation by opposition to a biaxial strain relaxation [25]. This process thus initiates at the damage peak by a change in the irradiation-defects nature from small defect clusters to extended defects (such as dislocations), which is a classical plastic relaxation mechanism. At the damaged/pristine interface, which is located far from the damage peak, the defect-creation rate is low and defects most likely accumulate there as a form of point defects. Furthermore, the crystalline registry is firmly preserved at the interface (at least in the fluence range investigated in this work). This property is most likely a characteristic of single-crystals. It is worth mentioning that, although there cannot be any shear strain under biaxial stress state for the {100} and {111} directions [7], such particular structure of single-crystals, where there is no interaction between grains of different orientation, could hamper shear strain to develop, contrary to what was measured in specific grain orientations in polycrystalline implanted UO_2 [7]. Both characteristics (low defect-formation rate and crystalline registry) may explain why the elastic strain keeps on increasing at the irradiated/virgin interface, at least until the material cannot sustain anymore the stored elastic energy, *i.e.* until the point-defect density is so high that extended defects also form in this region.

It is worth mentioning that this strain relaxation phenomenon occurs at the same dpa level in UO_2 irradiated with 500-KeV Ce (this work) as in ZrO_2 irradiated with 300-KeV Cs [26], *i.e.* in very similar irradiation conditions in terms of nuclear energy loss and damaged

thickness. It takes place at ~6 dpa for UO_2 and at ~5.1 dpa for ZrO_2 (this value has been recalculated as compared to that found in [26] by using same E_d values than those employed here for urania), so at a very similar dpa level. However, at this dose, the strain level – the total strain, which is that actually experienced by the crystals - at the damage peak is different for the two materials: ~1.1% (~1.7%) and ~0.8% (~1.25%) for {111}- and {100}-oriented UO_2 (ZrO_2), respectively. Since elastic properties of both materials are equivalent, this finding could be due to different primary irradiation defects. Both materials sharing the same crystallographic structure, one possible difference in the defect configuration and/or nature could lie in the charge of the defects since U has a larger flexibility in terms of oxidation state than Zr. Also, even if the defects were identical in the two materials, they could induce a different distortion field due to the presence of yttrium and associated native vacancies in yttria-stabilized zirconia; in other words, same defects could have a different so-called defect relaxation volume. To support these assumptions, one may note that similarities and differences between primary irradiation defects and their clustering properties have been recently pointed out by different computational methods in zirconia (with and without yttria), ceria and urania [27-28].

Conclusion

UO_2 single crystals with two different orientations, namely {111} and {100}, were irradiated in the nuclear energy-loss regime with 500-keV Ce^{3+} ions. Ce being totally soluble in urania, only collision cascade led to microstructural changes (no Ce bubble or Ce-based precipitates are expected to form). These changes were identified through the monitoring of the irradiation-induced strain using HRXRD; a mechanical modelling dedicated to thin irradiated layers was applied to account for the reaction of the unirradiated part of the

crystals. The elastic strain is found to be located along the surface normal of the samples (there is no in-plane strain), and it increases with fluence until it significantly relaxes. This behaviour is observed for both orientations, but the measured elastic strain depends on the crystallographic direction. Nevertheless, it is demonstrated that the strain due to irradiation defects only is equal for both directions. This result shows the necessity to use an adapted mechanical model for these irradiation conditions. Additionally, it indicates that, due to the isotropic nature of collisions cascades, defects of the same type and of equal concentration are formed in irradiated UO_2 in the two probed crystallographic directions. At same irradiation fluence for both orientations, a plastic deformation mechanism that initiates at the damage peak takes place to relieve the elastic strain. However, the in-plane lattice parameter of the irradiated layer remains unchanged and equal to that of the pristine material owing to the very strong damaged/pristine interface coherency. Meanwhile, the strain at this interface continues to increase.

Acknowledgements

We are grateful to the Semiramis staff for their help during irradiations. One of us (T.H. Nguyen) acknowledges the Ecole Doctorale MIPEGE at the Université Paris-Sud for financial support during his PhD thesis.

References

[1] Y. Serruys, M.-O. Ruault, P. Trocellier, S. Henry, O. Kaïtasov, Ph. Trouslard, NIM B 240 (2005) 124.

[2] L. Thomé, J. Jagielski, F. Garrido, Europhys. Lett., 47 (1999) 203.

[3] Th. Wiss, J.-P. Hiernaut, D. Roudil, J.-Y. Colle, E. Maugeri, Z. Talip, A. Janssen, V. Rondinella, R. J.M. Konings, H.-J. Matzke, W. J. Weber, J. Nucl. Mater. 451 (2014) 198.

[4] Y. Zhang, A. Debelle, A. Boulle, P. Kluth, F. Tuomisto, Curr. Opin. Sol. St. Mat. Sc. 19 (2015) 19.

[5] A. Debelle, A. Declémy, Nucl. Instr. Meth. B, 268 (2010) 1460.

[6] A Debelle, A Boulle, F Rakotovao, J Moeyaert, C Bachelet, F Garrido, L Thomé, J. Phys. D: Appl. Phys. 46 (2013) 045309.

[7] A. Richard, H. Palancher, E. Castelier, J.-S. Micha, M. Gamaleri, G. Carlot, H. Rouquette, Ph. Goudeau, G. Martin, F. Rieutord, J.-P. Piron, Ph. Garcia, J. Appl. Crystal. 45 (2012) 826.

[8] G. Velisa, A. Debelle, L. Vincent, L. Thomé, A. Declemy, D. Pantelica, J. Nucl. Mater. 402 (2010) 87.

[9] A. Debelle, A. Boulle, F. Garrido, L. Thomé, J. Mater. Sc. 46 (2011) 4683.

[10] F. Garrido, L. Vincent, L. Nowicki , G. Sattonnay, L. Thomé, NIM B 266 (2008) 2842.

[11] T.H. Nguyen, F. Garrido, A. Debelle, S. Mylonas, L. Nowicki, L. Thomé, J. Bourçois, J. Moeyaert, Nucl. Instr. Meth. B 326 (2014) 264.

[12] S. Moll, L. Thomé, G. Sattonnay, A. Debelle, F. Garrido, L. Vincent, J. Jagielski, J. Appl. Phys. 106, (2009) 073509.

[13] A. Debelle, J. Channagiri, L. Thomé, B. Décamps, A. Boulle, S. Moll, F. Garrido, M. Behar, J. Jagielski, J. Appl. Phys 115 (2014) 183504.

[14] Y. Miao, D. Aidhy, W.-Y Chen, K. Mo, A. Oaks, D. Wolf, J. F. Stubbins, J. Nucl. Mater. 445 (2014) 209.

[15] L.-F. He, M. Gupta, Cl. A. Yablinsky, J. Gan, M. A. Kirk, X.-M. Bai, J. Pakarinen, T. R. Allen, J. Nucl. Mater. 443 (2013) 71.

[16] L. Nowicki, A. Turos, R. ratajczak, A. Stonert, F. Garrido, Nucl. Instr. Meth. B 240 (2005) 277.

[17] Tien-Hien Nguyen, Ph.D. thesis: "Channelling investigation of the behaviour of urania under low-energy ion irradiation", Université Paris-Sud (2013), http://hal.in2p3.fr/tel-00966967/document.

[18] F. Garrido, L. Nowicki, L. Thomé, Phys. Rev. B 74 (2006) 184114.

[19] J.F. Ziegler, J. P. Biersack, U. Littmark, The Stopping and Range of Ions in Solids, Pergamon, New York, 1985. Available at: www.srim.org.

[20] A. Boulle, A. Debelle, J. Appl. Cryst. 43 (2010) 1046.

[21] J. B. Jr Wachtman, M. L. Wheat, H. J. Anderson, J. L. Bates, J. Nucl. Mater. 16 (1965) 39.

[22] H. Heinke, M. O. Möller, D. Hommel, G. Landwehr, J. Cryst. Growth 135 (1994) 41.

[23] S. Autier-Laurent, O. Plantevin, Ph. Lecoeur, B. Décamps, A. Gentils, C. Bachelet, O. Kaitasov, G. Baldinozzi, Europhys. Lett. 92 (2010) 36005.

[24] A. Debelle, A. Boulle, A. Chartier, F. Gao, W. J. Weber, Phys. Rev. B 90 (2014) 174112.

[25] F Conchon, A Boulle, R Guinebretiere, E Dooryhée, J-L Hodeau , C Girardot , S Pignard , J Kreisel, F Weiss, J. Phys. Condens. Matter 20 (2008) 145216.

[26] A. Debelle, A. Declémy, L. Vincent, F. Garrido, L. Thomé, J. Nucl. Mater. 396, (2010) 240.

[27] D. S. Aidhy, D. Wolf, A. El-Azab, Scripta Mater. 65 (2011) 867.

[28] D. S. Aidhy, Y. Zhang, W. J. Weber, Scripta Mater. 98 (2015) 16.

Figure captions

Figure 1: SRIM-predicted dpa (left axis) and Ce (right axis) depth profiles in 500-keV Ce-irradiated UO_2 at a fluence of $9x10^{14}$ cm^{-2}.

Figure 2: ω-2θ experimental scans (dots) recorded (a) in the vicinity of the 400 reflection and (b) in the vicinity of the 222 reflection for UO_2 single-crystals irradiated with 500-keV Ce^{3+} ions at indicated fluences expressed in cm^{-2}. Curves are shifted vertically for visualization purposes. The intensity is plotted on a logarithmic scale. Definition of the different axes is given in the text. Solid (red) lines are best fits with a dedicated simulation program [20].

Figure 3: Strain depth profiles obtained from the fitting of XRD curves presented in Fig1. Ion fluence increases from bottom to top, and the same colour code as in Fig.1 is used: 10^{14} cm^{-2}, (purple), $3x10^{14}$ cm^{-2} (blue), $5x10^{14}$ cm^{-2} (green), $7x10^{14}$ cm^{-2} (orange) and $9x10^{14}$ cm^{-2} (red). Dashed lines indicate that elastic strain cannot be precisely determined in this region because the irradiated layer is too defective (for more details, see text and [13]).

Figure 4: Variation as a function of both the Ce fluence and the dpa scale of the maximum of the total elastic strain ε^{tot} (full symbols), and the strain due to defects only ε^{def} (open symbols) determined in irradiated UO_2 crystals. Strain levels are presented for both {100} (black squares) and {111} (red circles) directions. Lines are drawn for visualization purposes.

Figure 5: XRD reciprocal space maps recorded in the vicinity of the asymmetric 331 reflection of {111}-oriented UO_2 crystals irradiated with 500-keV Ce^{3+} ions at (a) $3x10^{14}$ cm^{-2} and (b) $9x10^{14}$ cm^{-2}. Intensity is plotted in logarithmic scale; colour range varies from purple to red as intensity increases, and grey colour corresponds to the highest intensity level. The grey horizontal dotted lines indicate where line scans presented in Fig. 6 were taken.

Figure 6: Thin solid lines correspond to $K_{//}$ line scans at K_N = 7.331 nm^{-1} extracted from RSMs presented in Figs. 5 (see grey horizontal dotted lines in this figure). Thick solid lines represent best-fits with a pseudo-Voigt function.

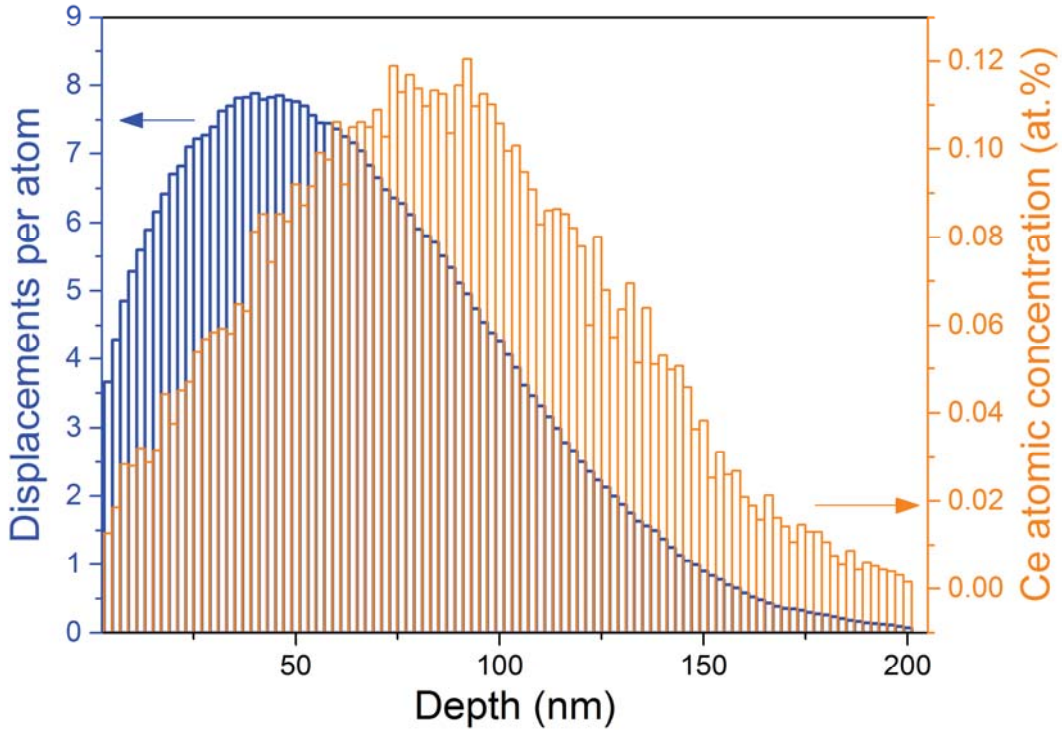

Figure 1

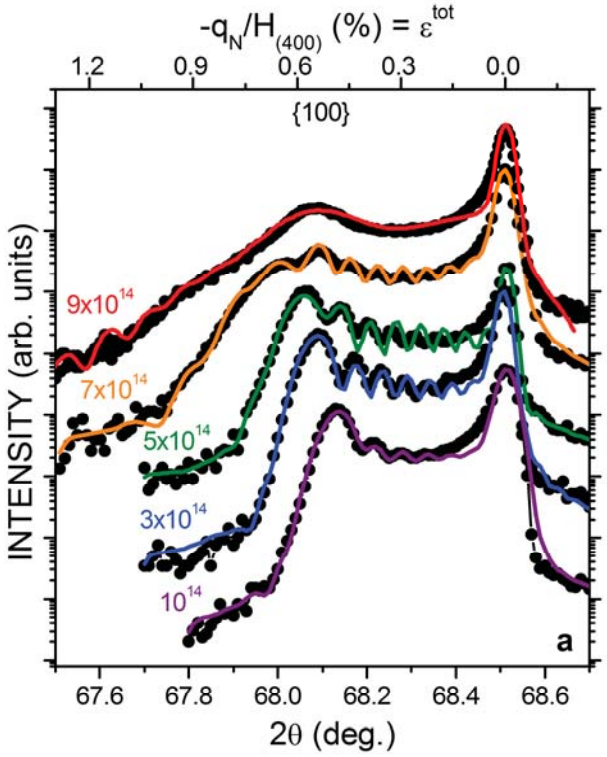

FIGURE 2a

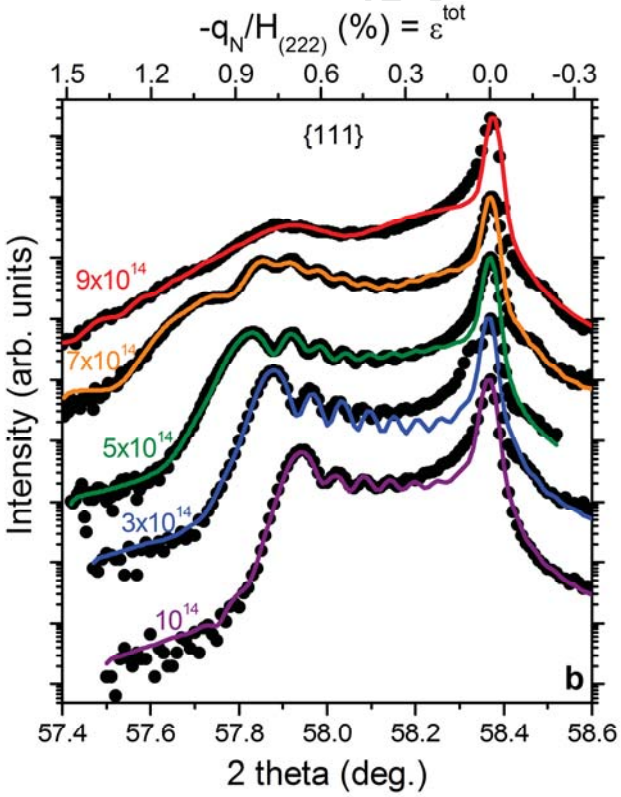

FIGURE 2b

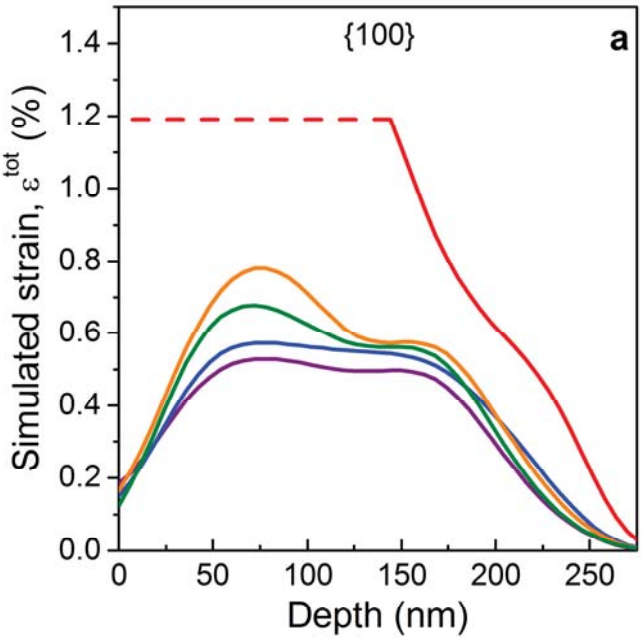

Figure 3a

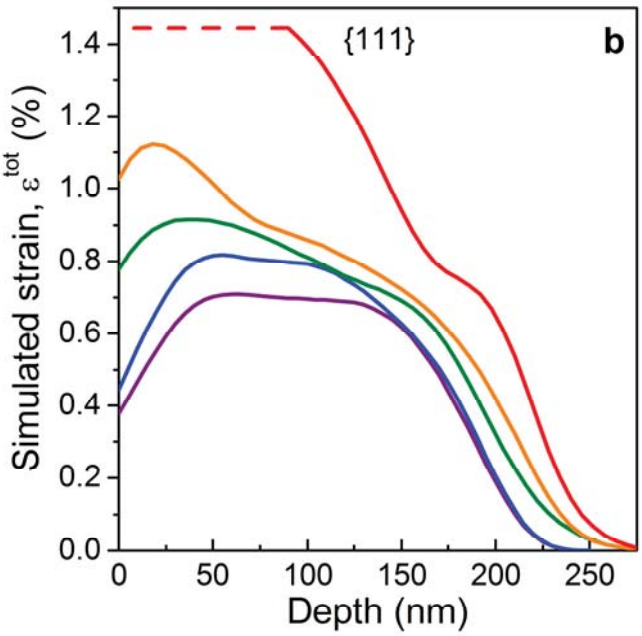

Figure 3b

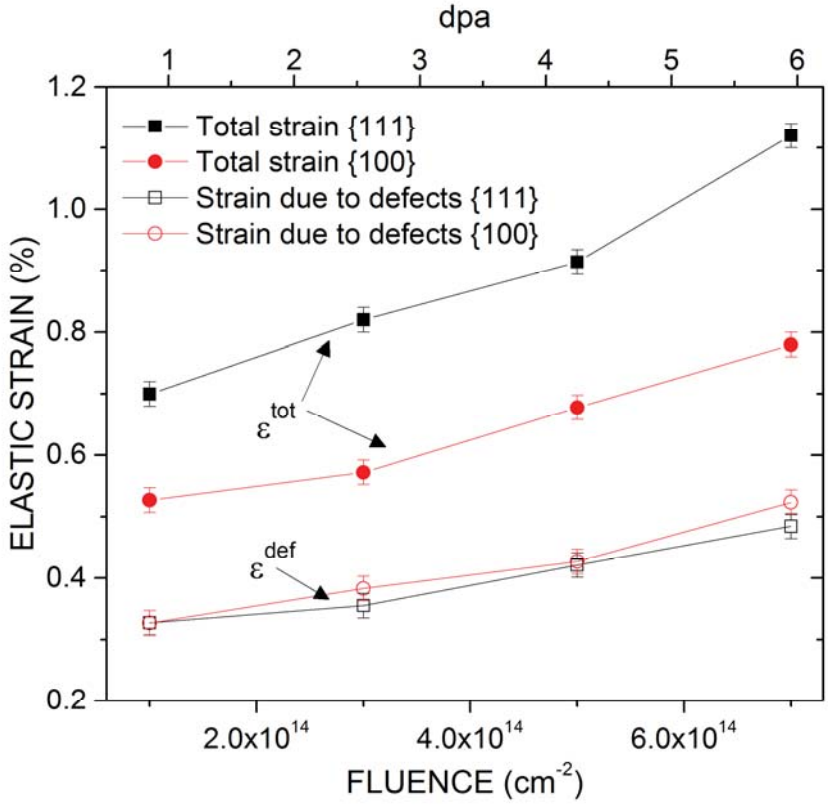

FIGURE 4

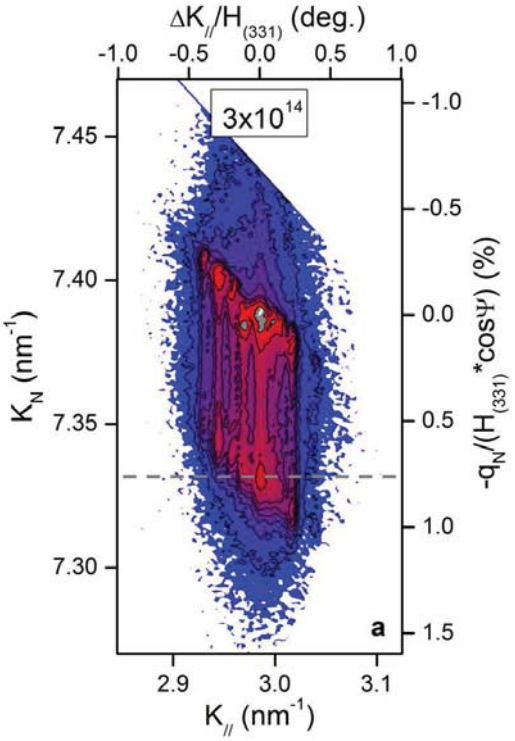

FIGURE 5a

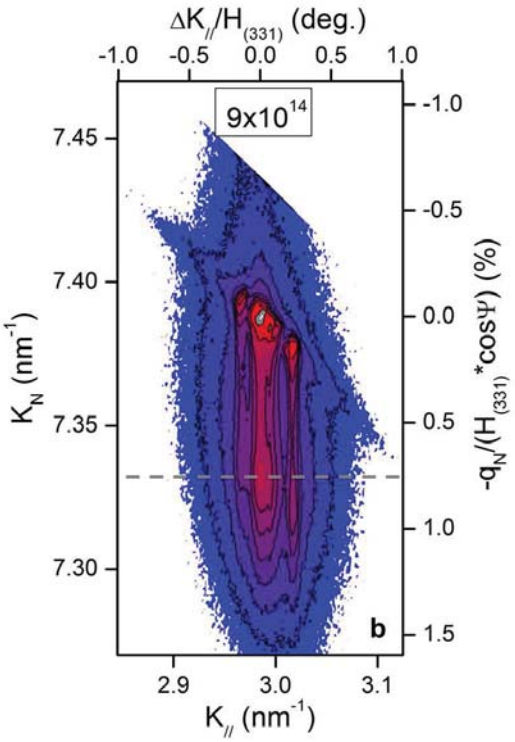

FIGURE 5b

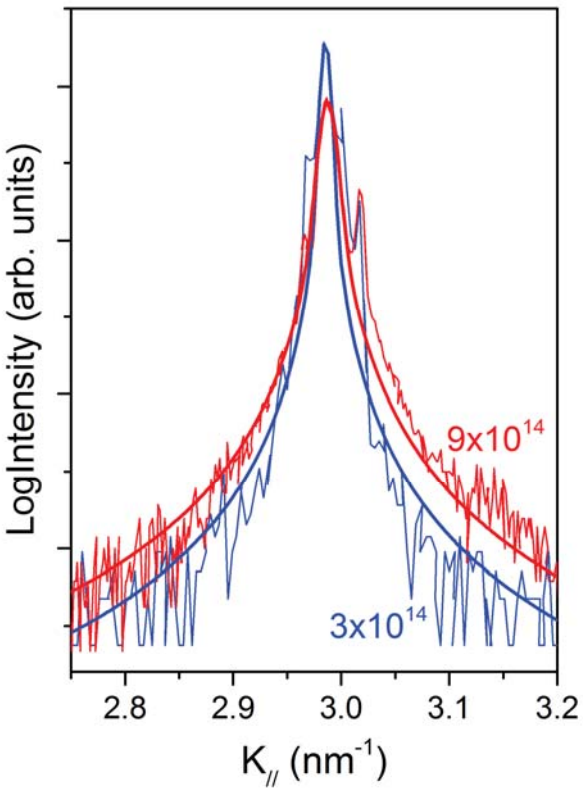

Figure 6